Direct and indirect excitons in semiconductor coupled quantum wells in an applied electric field

K. Sivalertporn, L. Mouchliadis,* A. L. Ivanov, R. Philp, and E. A. Muljarov†
School of Physics and Astronomy, Cardiff University, The Parade, Cardiff CF24 3AA, United Kingdom
(Received 11 November 2011; published 17 January 2012)

An accurate calculation of the exciton ground and excited states in AlGaAs and InGaAs coupled quantum wells (CQWs) in an external electric field is presented. An efficient and straightforward algorithm of solving the Schrödinger equation in real space has been developed and exciton binding energies, oscillator strengths, lifetimes, and absorption spectra are calculated for applied electric fields up to 100 kV/cm. It is found that in a symmetric 8–4–8-nm GaAs/$Al_{0.33}Ga_{0.67}$As CQW structure, the ground state of the system switches from direct to indirect exciton at approximately 5 kV/cm with dramatic changes of its binding energy and oscillator strength while the bright excited direct-exciton state remains almost unaffected. It is shown that the excitonic lifetime is dominated either by the radiative recombination or by tunneling processes at small/large values of the electric field, respectively. The calculated lifetime of the exciton ground state as a function of the bias voltage is in a quantitative agreement with low-temperature photoluminescence measurements. We have also made freely available a numerical code for calculation of the optical properties of direct and indirect excitons in CQWs in an electric field.

DOI: 10.1103/PhysRevB.85.045207 PACS number(s): 71.35.Cc, 73.21.Fg, 78.67.De, 72.20.Jv

I. INTRODUCTION

The electronic and optical properties of quantum-well structures have been widely investigated in the past decade due to their potential applications in electro-optic and opto-electronic devices. In recent years there has been growing interest in coupled quantum wells (CQWs) due to formation of long-lived excitons when these structures are placed in an electric field (EF). Intensive studies of indirect excitons in CQWs have resulted in their electrostatic and optical control.[1–7] Very recently, CQWs have been embedded into Bragg-mirror microcavities and there has been found a special type of voltage-tuned exciton polaritons which can be used for optical nonlinearities and polariton lasing achieved at much lower threshold powers.[8]

A CQW structure consists of two quantum wells separated by a barrier layer. For a sufficiently thin barrier, the tunneling of carriers through the barrier makes the two wells electronically coupled to each other. As a result, an electron (hole) can either reside in one of the two wells or its wave function (WF) is distributed between both wells. In the case of Coulomb bound electron and hole residing in the same well, they form a direct exciton. If, however, they are located in different wells, an indirect exciton is created.

In a symmetric CQW structure with no EF applied, formerly degenerate single-particle states split, due to the tunneling through the middle barrier, into doublets with symmetric and antisymmetric states in each. Since only transitions between states having the same parity are optically allowed, the Coulomb-coupled electron-hole (e-h) pairs form excitonic states that are optically either bright or dark. An EF, being applied in the growth direction, breaks down the symmetry of the system making all these excitons bright. In fact, single-particle states experience with EF a transition from states with well-defined parity to the ones with the electron (hole) located in one of the two wells, thus forming direct and indirect combinations of uncorrelated e-h pair states. These different pair states are Coulomb coupled with each other and form an exciton in which direct or indirect pair can dominate. In particular, with increasing EF, the exciton ground state (GS) undergoes a transition from bright direct exciton to indirect exciton which has a much weaker optical activity. The exciton radiative lifetime increases due to a reduction in the spatial overlap between the electron and hole WFs.[9–13] The exciton binding energy, in turn, reduces due to an increased e-h separation. It has also been found that the electronic coupling between quantum wells considerably enhances the quantum-confined Stark effect in CQW structures.[14–17] The tunneling effect is also enhanced with the EF allowing the carriers to leak out of the system.[18,19] This can lead to a considerable shortening of the photoluminescence decay time.[20] All these properties of CQWs make them a much richer system compared to single quantum wells.

Excitonic states in CQWs in the presence of EF have been intensively studied in recent years. Different theoretical approaches have been used ranging from variational methods[21–27] to direct diagonalizations in which the exciton WF is expanded into a large basis[28] or the Schrödinger equation is discretized in the momentum space.[29] In this paper, we present a more accurate and straightforward way for solving the Schrödinger equation for an exciton in a CQW structure. Expanding the exciton WF into e-h pair states we solve in the real space a system of differential equations for the exciton in-plane motion, using the shooting method, here generalized to a matrix form. The e-h pair basis states are calculated exactly using the analytical form of the electron (hole) WF in a uniform EF. We present the full calculation of exciton bound and (discretized) continuum states as well as the absorption spectrum of a CQW in an applied EF. We study the EF effect on the exciton binding energy and lifetime in a 8-4-8-nm GaAs/$Al_{0.33}Ga_{0.67}$As symmetric CQW structure, both for the ground and excited states, and demonstrate a direct-to-indirect crossover of the exciton ground state with increasing EF. An example of an asymmetric 10-4-10-nm InGaAs CQW having different In content in the left and right QWs is also given, demonstrating our calculation of the electron and hole energies of quantization and the exciton

transition energies and oscillator strengths as functions of the applied EF.

II. FORMALISM AND NUMERICAL METHOD

Let us consider a symmetric GaAs/$Al_xGa_{1-x}As$ CQW that consists of two GaAs QW layers separated by a thin $Al_xGa_{1-x}As$ barrier and surrounded on both sides by thick barriers of the same kind. In this paper we mainly concentrate on a CQW structure that has been intensively used in a series of experiments,[1–4,30] taking the barrier and well widths to be $L_b = 4$ nm and $L_w = 8$ nm, respectively, and the barrier concentration of Al to be $x = 0.33$. The electric field F is applied in the growth direction. For a different CQW in the presence of an EF simulations can be performed using our online available numerical code[31] (see Sec. III D below for more details). We are interested in optically allowed transitions in such a system and, thus, consider excitonic states with zero in-plane and angular momenta only. In the effective mass approximation, the excitonic Hamiltonian can be divided into three parts: the first two, $\hat{H}_e$ and $\hat{H}_h$, take into account the electron and hole quantization in heterostructure potentials V_e and V_h and the third one, $\hat{H}_X$, is responsible for the e-h in-plane relative motion and Coulomb binding,

$$\hat{H}(z_e,z_h,\rho) = \hat{H}_e(z_e) + \hat{H}_h(z_h) + \hat{H}_X(z_e,z_h,\rho) + E_g \quad (1)$$

with

$$\hat{H}_{e,h}(z) = -\frac{\hbar^2}{2}\frac{\partial}{\partial z}\frac{1}{m_{e,h}(z)}\frac{\partial}{\partial z} + V_{e,h}(z) \pm eFz, \quad (2)$$

$$\hat{H}_X = -\frac{\hbar^2}{2\mu}\left(\frac{\partial^2}{\partial\rho^2} + \frac{1}{\rho}\frac{\partial}{\partial\rho}\right) - \frac{e^2}{\varepsilon_b\sqrt{(z_e - z_h)^2 + \rho^2}}, \quad (3)$$

where $z_{e(h)}$ is the electron (hole) coordinate in the growth direction, ρ the coordinate of the e-h relative motion in the QW plane, ε_b the background dielectric constant that we assume to be z independent, m_e the electron effective mass, and E_g the band gap of the well material (GaAs). Due to the strong QW confinement, the heavy-hole subband is split off considerably and can be approximated by an anisotropic effective mass using the Kohn-Luttinger parameters γ_1 and γ_2,[32]

$$\frac{1}{m_h} = \frac{1}{m_0}(\gamma_1 - 2\gamma_2), \quad (4)$$

$$\frac{1}{\mu} = \frac{1}{m_e} + \frac{1}{m_0}(\gamma_1 + \gamma_2), \quad (5)$$

where m_h is the hole effective mass in the growth direction, μ the exciton in-plane reduced mass, and m_0 the free electron mass. We assume a rectangular form of the heterostructure confinement potentials,

$$V_{e,h}(z) = \begin{cases} 0 & \text{inside the wells,} \\ \mathcal{V}_{e,h} > 0 & \text{outside,} \end{cases} \quad (6)$$

and similar steplike profiles for the electron and hole effective masses in the growth direction.

In our calculation, we have used the following parameters: the background dielectric constant[24] $\varepsilon_b = 12.5$, the energy-band offset ratio[29] $\mathcal{V}_e$:$\mathcal{V}_h$ = 65:35. The band gap discontinuity at the GaAs/$Al_xGa_{1-x}As$ interface is linearly approximated[24] as $1.247x$ eV. The Kohn-Luttinger parameters for pure GaAs and AlAs are obtained from Ref. 33: $m_e = 0.0665\ m_0$, $\gamma_1 = 6.79$ and $\gamma_2 = 1.92$ in GaAs (giving the hole mass $m_h = 0.34\, m_0$); and $m_e = 0.15\, m_0$, $\gamma_1 = 3.79$ and $\gamma_2 = 1.23$ in AlAs (giving $m_h = 0.75\ m_0$). The $Al_xGa_{1-x}As$ alloy parameters were linearly interpolated between those of GaAs and AlAs. In particular, for the content $x = 0.33$, we have used $m_e = 0.094\ m_0$ and $m_h = 0.48\ m_0$ in $Al_{0.33}Ga_{0.67}As$ layers. The in-plane reduced mass in the barrier layers ($0.057\ m_0$) differs from that in the well layers ($0.042\ m_0$). However, because of a very small probability for the exciton ground state to find the carriers in the barrier, we take for the in-plane reduced mass the GaAs value of $\mu = 0.042\ m_0$.

A. Electron and hole single-particle states

To solve the excitonic Schrödinger equation with the full Hamiltonian Eq. (1) we, first, prepare a basis of single-particle states that satisfy the following one-dimensional equations:

$$\hat{H}_{e,h}(z)\psi^{e,h}(z) = E^{e,h}\psi^{e,h}(z). \quad (7)$$

To do so, we use the advantage of the analytic form of the electron and hole WFs in the rectangular confinement potentials Eq. (6) and uniform electric field F. In each layer of the CQW structure, the electron WF is given by a superposition of two Airy functions[34]

$$\psi^e(z) = a_k\mathrm{Ai}(\xi) + b_k\mathrm{Bi}(\xi), \quad (8)$$

where

$$\xi(z) = \left(\frac{2m_e eF}{\hbar^2}\right)^{1/3}\left[z - \frac{E^e - V_e(z)}{eF}\right] \quad (9)$$

and the index k labels the heterostructure layers (from left to right), taking integer values from 1 to 5. The electron eigenenergy E^e and five pairs of coefficients (a_k, b_k) in Eq. (8) are found from four pairs of boundary conditions (BCs) on heterostructure interfaces and two BCs at $z \to \pm\infty$.

The interface BCs following from Eqs. (2) and (7) are the continuity of $\psi^e(z)$ and $m_e^{-1}(z)\partial\psi^e(z)/\partial z$. The other two BCs take into account the possibility for the electron to tunnel through the barrier and escape from the system to the side of the CQW structure where the applied EF gradually lowers the potential. In that area, the solution is given by a wave propagating away from the system. For the electron WF and $F > 0$, this outgoing BC at $z \to -\infty$ yields $b_1 = -ia_1$, which follows from the specific combination of the Airy functions $\mathrm{Ai}(\xi) - i\mathrm{Bi}(\xi)$, producing an outgoing wave.[18,34] At the same time, the electron cannot escape to the other side of the structure where the potential gradually increases, and, thus, the other BC, typical for bound/localized states, is $\psi^e(z \to +\infty) = 0$, giving $b_5 = 0$ due to the asymptotics of the Airy functions.[34] The form of the WF and the BCs for the hole are found in a similar way, taking into account that the potential grows in the opposite direction. The secular equation following from all 10 BCs determines discrete eigenvalues of Eq. (7),

$$E_j^{e,h} = \tilde{E}_j^{e,h} - i\Gamma_j^{e,h}, \quad (10)$$

which are the complex energies of electron/hole resonant states, also known in the literature as Siegert states.[35] The

real part of the eigenvalue, $\tilde{E}_j^{e(h)}$, is the energy position of the electron (hole) j-th resonant level, while the imaginary part $\Gamma_j^{e(h)}$ gives its tunneling linewidth.

The WF of any resonant state having a finite linewidth is essentially complex, i.e., it cannot be made real by any uniform phase shift. Also, its amplitude grows exponentially to the outside area to which the particle can escape and, thus, has to be normalized to its flux.[35,36] This normalization includes a divergent volume integral and a compensating surface term. For the values of the EF considered in this paper, the calculated linewidths of the electron and hole states of interest are always small compared to their energies of quantization. Similarly, the imaginary parts of the WFs are small compared to the real ones and can be dropped. The normalization condition is then taken in a form

$$\int_{z_{\min}}^{z_{\max}} \left[\tilde{\psi}_j^{e,h}(z)\right]^2 dz = 1, \tag{11}$$

where $\tilde{\psi}_j^{e,h} = \mathrm{Re}(\psi_j^{e,h})$. The limits of integration in Eq. (11), $z_{\min}$ and $z_{\max}$, taken to be the same for electron and hole, are two distant points on both sides of the CQW where the WFs decay considerably before they start to grow exponentially due to the carrier tunneling, so the surface terms are minimized and can be dropped leaving in the normalization only finite-volume integrals.

Different electron and hole subbands ($\tilde{E}_i^e$ for $i = 1,2$ and $\tilde{E}_j^h$ for $j = 1$–4) calculated in the presence of the EF are shown in Fig. 1. The corresponding WFs, $\tilde{\psi}_i^e$ and $\tilde{\psi}_j^h$, are illustrated in Figs. 2(a)–2(d) for a few different values of the EF. At zero field, the GS and the first ES have, respectively, symmetric and antisymmetric WFs; see Fig. 2(a). With increasing EF, the WFs become asymmetric, and the WF maxima for the electron and hole GSs move in opposite directions. The GS and the first ES for the same carrier are also confined in different QWs. This happens to both carriers already at $F = 2\,\mathrm{kV/cm}$; see Fig. 2(b). As the EF grows further, the GS-ES splittings increase almost linearly with F (Fig. 1), and the hole ES jumps from the left to the right QW [Fig. 2(c)]. This corresponds to an anticrossing of hole ES subbands that takes place at 27.8 kV/cm; see the inset in Fig. 1(b). Such an anticrossing behavior was also found in previous calculations.[23,29] The same happens to the electron ES at a much higher EF. Figure 2(d) shows a modified ES WF for $F = 100$ kV/cm that is a precursor of a similar transition for the electron.

Far from the CQW structure, we observe tiny oscillations in the WF of the electron (hole) GS in the left (right) barrier; see Figs. 2(e) and 2(f). This oscillatory behavior, typical for freely propagating particles, occurs due to the lowering of the potential by the EF, so an electron (hole) can escape to the left (right) barrier. Since $m_h V_h > m_e V_e$, the frequency of the oscillations for the hole is larger than that for the electron. Such oscillations become more dramatic and start earlier (closer to the CQW center) for some of higher ESs. For example, for $F = 100$ kV/cm the hole state $h3$ exibits huge oscillations clearly seen in Fig. 2(d). However, the next hole ES $h4$ which has the dominant contribution to the direct exciton state discussed below has only tiny oscillations, similar to those in Fig. 2(f), and a small tunneling rate, comparable to that of the hole GS.

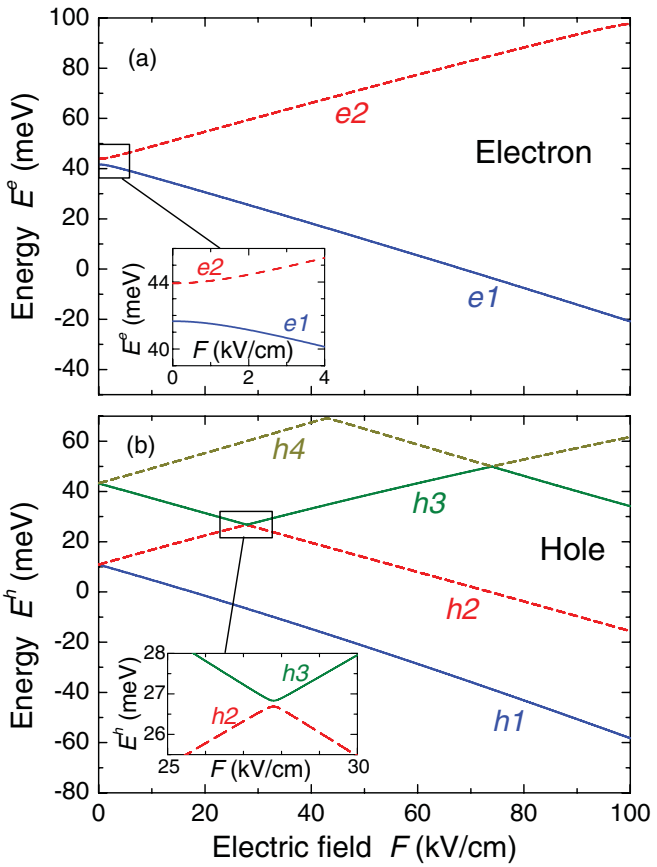

FIG. 1. (Color online) Energies of two electron states (a) and four hole states (b) in 8–4–8-nm GaAs/$Al_{0.33}Ga_{0.67}As$ CQW as functions of an applied electric field. Insets show spectral regions with anticrossing.

B. Excitonic states: Multi-sub-level approach

We calculate excitonic states in a CQW structure in the presence of an EF, expanding the exciton WF into a finite set of e-h pair states,

$$\Psi(z_e, z_h, \rho) = \sum_{n=1}^{N} \Phi_n(z_e, z_h)\phi_n(\rho), \tag{12}$$

where

$$\Phi_n(z_e, z_h) = \tilde{\psi}_i^e(z_e)\tilde{\psi}_j^h(z_h), \quad n = (i, j), \tag{13}$$

and $\tilde{\psi}_i^{e,h}(z)$ are the electron and hole wave functions calculated in the presence of EF and heterostructure potentials; see Sec. II A. The Schrödinger equation for the exciton, $\hat{H}\Psi = E_X\Psi$, then takes the form

$$\left[\hat{K}(\rho) + E_n^{(0)} - E_X\right]\phi_n(\rho) + \sum_{m=1}^{N} V_{nm}(\rho)\phi_m(\rho) = 0 \tag{14}$$

with

$$\hat{K}(\rho) = -\frac{\hbar^2}{2\mu}\left(\frac{\partial^2}{\partial\rho^2} + \frac{1}{\rho}\frac{\partial}{\partial\rho}\right), \tag{15}$$

$$V_{nm}(\rho) = -\frac{e^2}{\varepsilon_b}\iint_{z_{\min}}^{z_{\max}} \frac{\Phi_n(z_e, z_h)\Phi_m(z_e, z_h)}{\sqrt{(z_e - z_h)^2 + \rho^2}}\, dz_e dz_h, \tag{16}$$

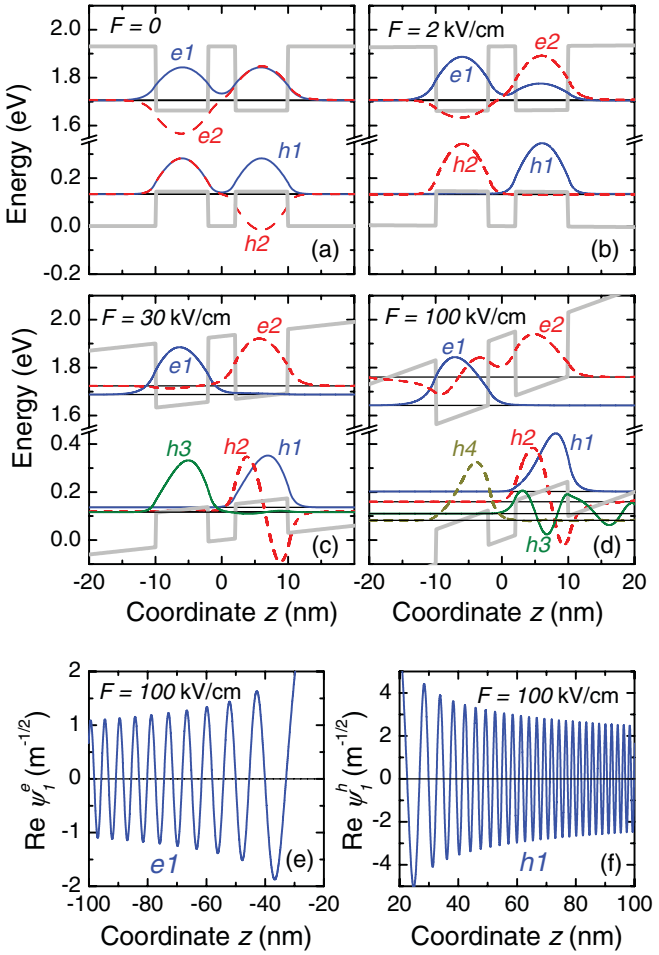

FIG. 2. (Color online) [(a)–(d)] Wave functions and energy levels of electron and hole ground and excited states for different values of the electric field F. Gray lines show CQW heterostructure potentials, using $E_g = 1.519$ eV for the band gap. [(e) and (f)] Oscillating tails in the electron and hole wave functions.

and the energies of pair states given by

$$E_n^{(0)} = \tilde{E}_i^e + \tilde{E}_j^h + E_g. \tag{17}$$

In our calculation of the exciton states in 8-4-8-nm GaAs/$Al_{0.33}Ga_{0.67}As$ CQW for EFs up to $F = 25$ kV/cm it was sufficient to restrict the basis in Eq. (12) to *four* e-h pair states ($N = 4$), keeping only the GS and the first ES for electron and hole. This allowed us to calculate the exciton GS with an accuracy better than 0.01 meV. We label these four basis states as $e1h1$ ($n = 1$), $e1h2$ ($n = 2$), $e2h1$ ($n = 3$), and $e2h2$ ($n = 4$), where e (h) stands for an electron (hole) and the numbers 1 and 2 refer to the single-particle GS and first ES, respectively, while n is the unified pair index introduced in Eq. (13). Other QW structures may require higher ESs to be taken into account. These are also needed in our case when a stronger EF is considered. In particular, higher quantized levels for the hole $h3$ and $h4$ [see Fig. 1(b)] are taken into account for $F >$ 25 kV/cm and $F > 70$ kV/cm, respectively, and these states have a major contribution to the direct exciton WF.

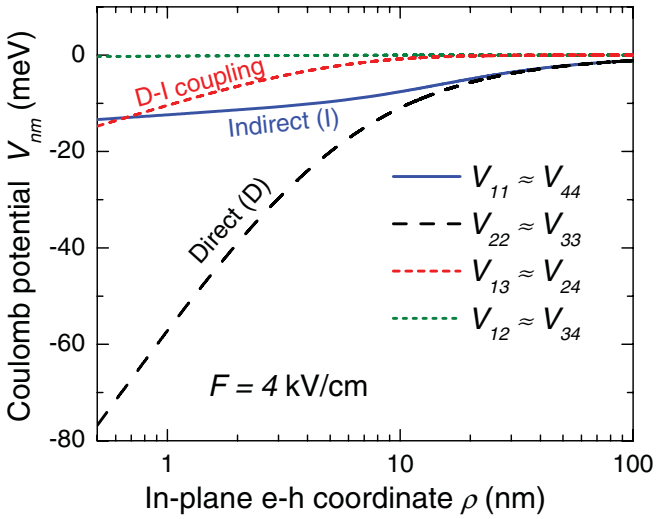

FIG. 3. (Color online) Matrix elements V_{nm} of the Coulomb potential calculated between different e-h pair states at $F = 4$ kV/cm.

We calculate the exciton transition energy E_X and the in-plane components of the WF, $\phi_n(\rho)$, by solving the matrix differential equation [Eq. (14)] numerically. To do so, we introduce a matrix generalization of the shooting method, applying the latter to a system of coupled differential equations. The shooting method transforms a boundary-value problem like Schrödinger's equation with BCs to an initial-value problem in which one of the boundary values (in the present case the WF at $\rho \to \infty$) is taken as a starting point. The boundary value(s) on the other side (at $\rho = 0$) is then used to find the eigenenergies. The BCs follow straightforwardly from Eq. (14) and the asymptotics of the Coulomb matrix elements $V_{nm}(\rho)$. At large distances $V_{nm}(\rho) \to -\delta_{nm}e^2/(\varepsilon_b\rho)$, while at small distances the potentials $V_{nm}(\rho)$ have logarithmic dependence, as is clear from Fig. 3. Therefore, for bound states

$$\phi_n(\rho \to \infty) = A_n \rho^{s_n} e^{-\alpha_n \rho}, \tag{18}$$

where $\alpha_n = \sqrt{2\mu(E_n^{(0)} - E_X)}/\hbar$ and $s_n = \mu e^2/(\hbar^2 \varepsilon_b \alpha_n) - 1/2$, and

$$\phi_n'(0) = 0\,. \tag{19}$$

Discretizing Eq. (14) on a finite grid, a numerical solution in the area $0 \leqslant \rho \leqslant R$ is generated iteratively using a finite difference scheme. In particular, a second-order scheme that we have used in our calculation brings Eq. (14) to the form

$$\phi_n(\rho - \Delta\rho) = -\phi_n(\rho + \Delta\rho)\frac{2\rho + \Delta\rho}{2\rho - \Delta\rho} + \sum_{m=1}^{N} F_{nm}(\rho)\phi_m(\rho), \tag{20}$$

where $\Delta\rho$ is the discretization step and the matrix $F_{nm}(\rho)$ depends on the Coulomb interaction and on a finite-difference representation of the kinetic term Eq. (15). The WF amplitudes A_n in the starting values $\phi_n(R)$ in Eq. (18) are the unknowns to be found along with the eigenvalue E_X. Going to the very

last point $\rho = 0$ and using the boundary condition Eq. (19) produces a homogeneous matrix equation of the form

$$\sum_{m=1}^{N} M_{nm}(E_X) A_m = 0 \tag{21}$$

in which $M_{nm}(E_X)$ depends solely on the exciton energy E_X (and no longer on ρ), and, thus, the energy eigenvalues are determined by

$$\det |M_{nm}(E_X)| = 0. \tag{22}$$

For small values of the EF, the electron and hole GS-ES splittings are smaller than the exciton Coulomb energy (compare Figs. 1 and 3) and, thus, several bound states [having the asymptotics given by Eq. (18)] can always be found in the system. However, as the EF grows, the Coulomb energy of the exciton ESs is getting smaller than the e-h pair splitting energies and, thus, some of these exciton states become unbound. Since the unbound states have energies $E_X > E_1^{(0)}$, at least for some of their radial components the asymptotics Eq. (18) is no longer valid and a proper treatment of the excitonic continuum is required. This task is outside the scope of the present paper, which mainly concentrates on exciton bound states. Nevertheless, some effects of the continuum and, in particular, its influence on the excitonic absorption spectrum can be taken into account, in a first attempt, by restricting the exciton in-plane motion to a large circle of radius R and in this way discretizing the continuum. The asymptotic boundary conditions Eq. (18) are now replaced by

$$\phi_n(R) = 0\,, \quad \phi_n(R - \Delta\rho) = A_n, \tag{23}$$

where the new amplitudes A_n satisfy the same Eq. (21) with matrix $M_{nm}(E)$ being redefined accordingly.

It is convenient to normalize the radial components of the WFs introducing expansion coefficients C_n:

$$\phi_n(\rho) = C_n \tilde{\phi}_n(\rho), \tag{24}$$

where $\tilde{\phi}_n(\rho)$ is normalized to $2\pi \int_0^\infty |\tilde{\phi}_n|^2 \rho d\rho = 1$ and, therefore,

$$\sum_{n=1}^{N} |C_n|^2 = 1, \tag{25}$$

due to orthogonality of the e-h pair states $\Phi_n(z_e, z_h)$ and normalization of the total exciton WF $\Psi(z_e, z_h, \rho)$.

Finally, for each excitonic state, the oscillator strength per unit area is calculated as[37]

$$f = \frac{2m_0 E_X |d_{cv}|^2}{\hbar^2} \left| \int_{z_{\min}}^{z_{\max}} \Psi(z, z, \rho = 0)\, dz \right|^2, \tag{26}$$

where d_{cv} is the basic dipole matrix element between the valence and conduction bands, and the overlap integral in Eq. (26) accounts for the spatial distribution of the excitonic recombination. The exciton radiative linewidth is then given by

$$\Gamma_R = \frac{\pi e^2 \hbar}{\sqrt{\varepsilon_b} m_0 c} f, \tag{27}$$

where c is the speed of light.

III. RESULTS AND DISCUSSION

In the presence of EF, the energy levels of the electron and hole single-particle states in a CQW structure experience Stark shifts $\tilde{E}_{1,2}^{e(h)}(F) \approx \tilde{E}_{1,2}^{e(h)}(0) \mp dF/2$ as demonstrated in Fig. 1, where $d = L_w + L_b$ is the center-to-center distance between the QWs. Concentrating on these two lowest levels for the electron and two for the hole we are, thus, dealing with four e-h pair states. For two of them, $e1h2$ and $e2h1$, the energies $E_{2,3}^{(0)}$ [see Eq. (17)] remain almost unaffected by the EF as the Stark shift for the electron is compensated by that for the hole, while the other two pair states, $e1h1$ and $e2h2$, have Stark shifts that are 2 times larger than the single-particle states: $E_{1,4}^{(0)}(F) \approx E_{1,4}^{(0)}(0) \mp dF$. Even though our CQW is symmetric, at nonzero EF the ground and the first excited single-particle states are localized in different wells of the CQW structure; see Fig. 2(b). That is why the pair states with electron and hole in the same QW ($n = 2$ and $n = 3$) are electrically neutral and can be called *direct* states while the other two, $n = 1$ and $n = 4$, with electron and hole in different QWs, have nonzero dipole moment and are called *indirect* states. As for excitonic states, they are, strictly speaking, neither direct nor indirect, since the exciton WF is always a combination of different pair states.

A. Crossover from direct to indirect exciton

In the absence of the Coulomb interaction, all four pair states are nearly degenerate at zero EF: Due to a rather weak tunneling through the middle barrier of the CQW, the energy splittings are small compared to the Coulomb energy (2.3 and 0.05 meV splitting for electron and hole, respectively, versus 4- to 9-meV binding energy). The Coulomb interaction splits further and strongly mixes the direct and indirect e-h pair states. To understand these splitting and mixing, let us consider the Coulomb matrix elements in more detail.

Figure 3 shows an example of the Coulomb matrix elements for $F = 4$ kV/cm, though this picture does not change much when the EF increases or decreases. The direct and indirect pair states have different charge separation, and, thus, their diagonal Coulomb matrix elements also differ markedly: Potentials $V_{22} \approx V_{33}$ for the direct pairs are a few times stronger than $V_{11} \approx V_{44}$ for the indirect ones. This difference brings in a considerable splitting between the direct and indirect pair states at $F = 0$: The indirect doublet is found almost 5 meV above the direct one; see Fig. 4. Among off-diagonal elements, the largest are $V_{13} \approx V_{24}$, due to a considerable overlap between the electron ground and excited states. All other matrix elements are two to three orders of magnitude smaller, because of a much larger effective mass of the hole and, consequently, much smaller overlap integrals. All off-diagonal elements drop quickly at large ρ due to the orthogonality of WFs.

The Coulomb coupling matrix elements $V_{13} \approx V_{24}$ are responsible for the mixing of direct and indirect pair states and, in particular, for a *crossover* of the ground exciton state from direct to indirect type as the EF grows. Due to this off-diagonal coupling, the Stark red-shifted indirect state $e1h1$ ($n = 1$) has a remarkable anticrossing with the direct pair state $e2h1$ ($n = 3$), weakly dependent on the EF. This anticrossing takes place at about $F = 5$ kV/cm and is clearly seen in

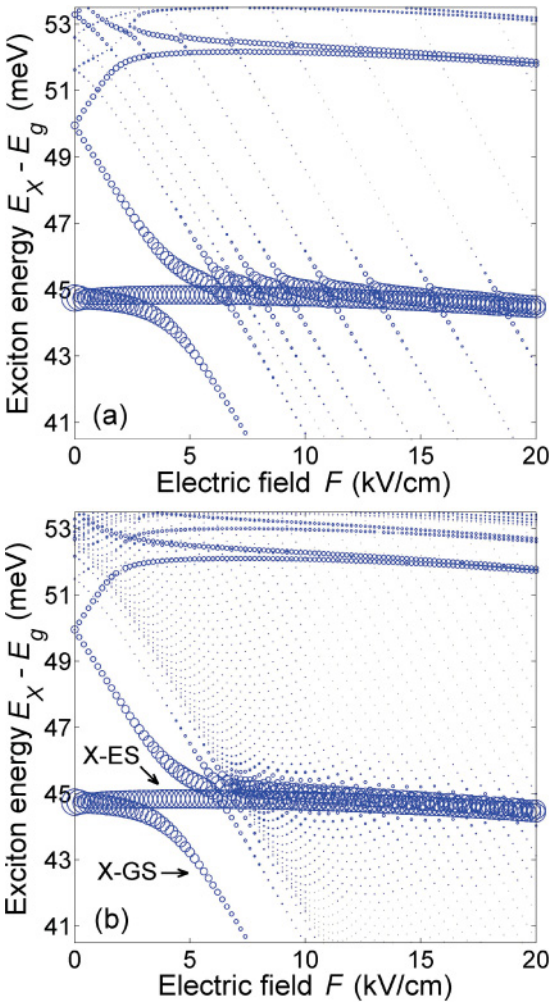

FIG. 4. (Color online) Electric field dependence of the optical transition energy E_X for different exciton states in a 8-4-8-nm GaAs/$Al_{0.33}Ga_{0.67}$As symmetric CQW structure, calculated using the exciton confinement radius $R = 200$ nm (a) and 800 nm (b). The circle area is proportional to the exciton oscillator strength f.

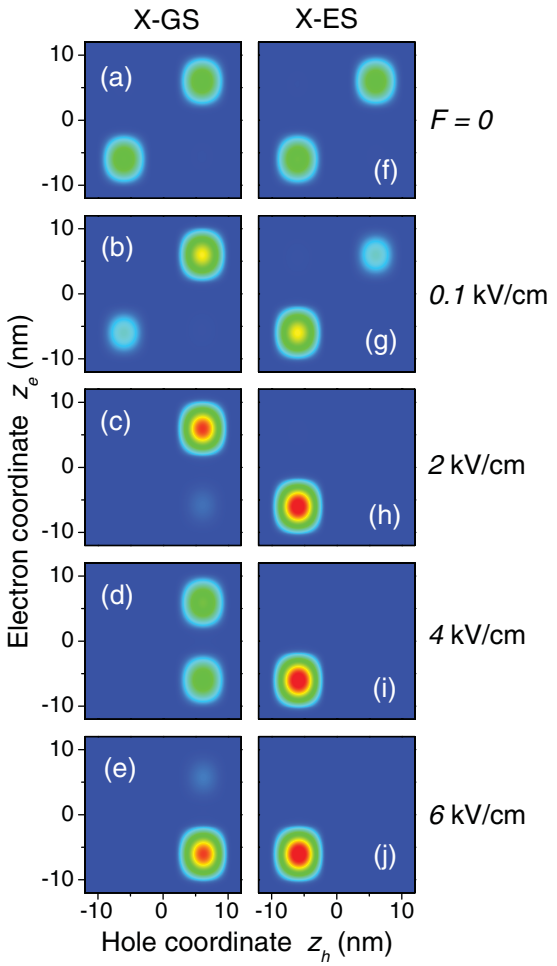

FIG. 5. (Color online) Probability distributions $\int_0^\infty |\Phi(z_e,z_h,\rho)|^2\, 2\pi\rho d\rho$ calculated for the exciton ground state X-GS [(a)–(e)] and excited state X-ES [(f)–(j)] for different values of the electric field.

Fig. 4. Indeed, the exciton ground state (X-GS) experiences a crossover from direct to indirect exciton: The oscillator strength of the X-GS has its maximum at $F = 0$ and then drops quickly with increasing EF as seen in Fig. 4. Since all other matrix elements including V_{12} are generally much smaller, the other direct pair state $e1h2$ ($n = 2$) remains unaffected and is only Coulomb shifted by the diagonal element V_{22}. Although it is strongly coupled via V_{24} to the other indirect state $e2h2$ ($n = 4$), the latter is Stark blue shifted and, thus, significantly detuned from $e1h2$ having a minor effect on it. As a result, the energy position of the brightest exciton excited state (X-ES), which has the maximum oscillator strength in the excitonic spectrum, remains practically unchanged.

The excitonic states shown in Figs. 4(a) and 4(b) are calculated with different in-plane exciton confinement radius, $R = 200$ nm and 800 nm, respectively [see Eq. (23)]. In the latter case the excitonic continuum has a much finer discretization that makes more clear which states belong to the continuum and which are the true bound states having more or less isolated positions, weakly dependent on R. For example, the $2S$ and $3S$ states of the indirect exciton are clearly identified in Fig. 4(b): They lie just below the discretized continuum onset and are down-shifted with F almost parallel to the exciton ground state. Higher excited states of the direct exciton are also well seen in Fig. 4: They are deep in the continuum (7–8 meV above the brightest direct state) and are weakly dependent on the EF.

Let us consider the properties of the X-GS and X-ES and, in particular, the direct-to-indirect (D-I) crossover in more detail. The contour plots in Fig. 5 show localization of the X-GS and X-ES across the CQW structure for different values of F. At zero EF, due to the symmetry of the system, both states have two identical maxima on the main diagonal $z_e = z_h$ [Figs. 5(a) and 5(f)], which refer to the direct nature of both excitonic states. With increasing EF one of the two peaks becomes smaller and then vanishes; see Figs. 5(b) and 5(c) and Figs. 5(g) and 5(h). The states become asymmetric, having both carriers localized either in the right QW (in X-GS) or in the left QW (in X-ES). Further increase of the EF up to $F = 6$ kV/cm leads to the X-GS switching from a direct to an indirect state: The peak moves away from the main diagonal

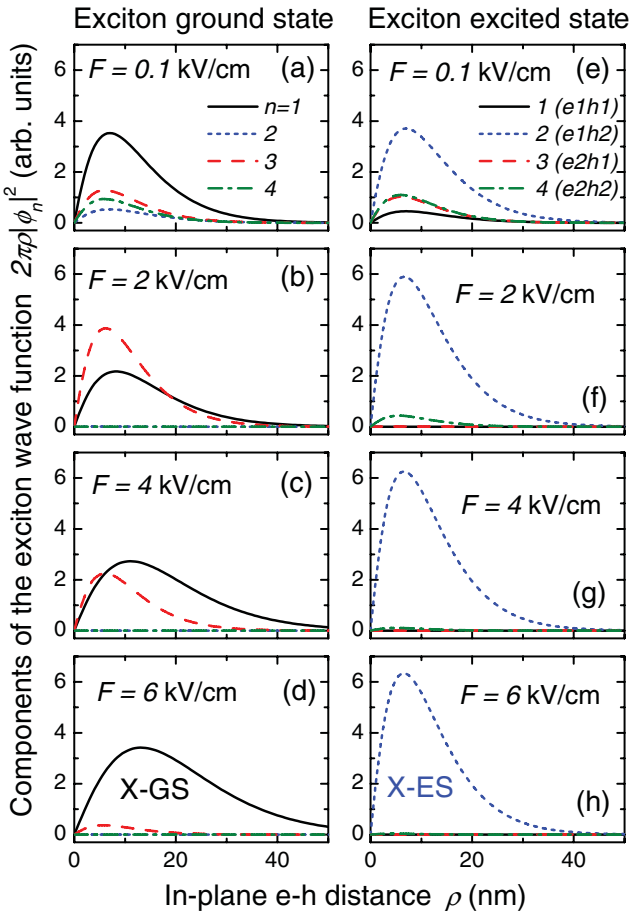

FIG. 6. (Color online) Radial components $2\pi\rho|\phi_n(\rho)|^2$ of the exciton wave function calculated for the ground state X-GS [(a)–(d)] and excited state X-ES [(e)–(h)] for different values of the electric field.

toward the bottom right corner; see Figs. 5(c)–5(e). This result is in good agreement with previous theoretical findings[28,29] and experimental observations.[30] At the same time the X-ES remains unchanged. The dominant hole component in the X-ES changes from $h2$ to $h3$ and from $h3$ to $h4$ when the system passes through the anticrossings of the hole levels at $F =$ 27.8 kV/cm and 74 kV/cm, respectively. The X-ES remains the brightest state in the excitonic spectrum having at the same time a very weak dependence on the EF that emphasizes its direct nature.

The D-I crossover of the X-GS is demonstrated also in Fig. 6 where different radial components $\phi_n(\rho)$ of the X-GS and X-ES WFs are plotted. At $F = 2$ kV/cm the direct e-h pair state $n = 3$ has the dominant contribution to the X-GS. This state is strongly coupled to the indirect pair state $n = 1$ via the Coulomb matrix element V_{13}, as discussed above. As a result of this anticrossing, ϕ_1 grows and ϕ_3 reduces with the EF. Nothing similar happens to the X-ES. The latter is always dominated by the $n = 2$ pair state which is coupled to the significantly detuned $n = 4$ state. Therefore, only a minor contribution of the ϕ_4 to the X-ES can be seen in Figs. 6(f)–6(h). The picture differs completely for smaller EFs. At $F = 0$ the symmetric $n = 1$ pair state is Coulomb coupled to the other symmetric state ($n = 4$), producing bright

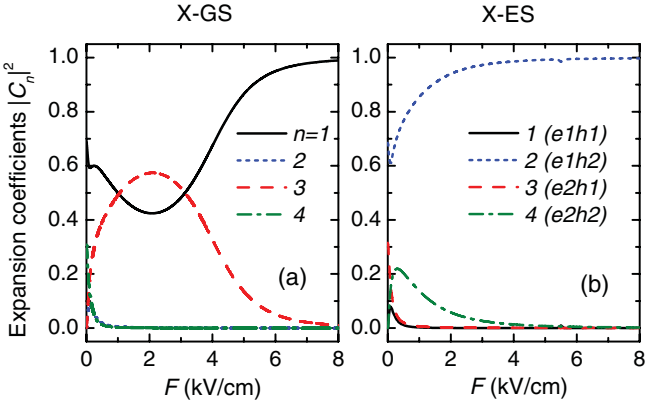

FIG. 7. (Color online) Coefficients C_n of the expansion of the exciton wave function into e-h pair states calculated for the ground state X-GS (a) and excited state X-ES (b) as functions of the electric field F.

X-GS and dark X-ES. These symmetric pair states do not interact with the antisymmetric states ($n = 2$ and 3) that are, in turn, coupled to each other. The transition from such symmetric coupling to the above considered D-I coupling has a rather narrow interval of small values of the EF and involves interaction of all four e-h pair states. In fact, for $F = 0.1$ kV/cm one can see in Figs. 6(a) and 6(e) that all four components have comparable contributions to the X-GS and X-ES WFs. Figure 7 summarizes our analysis showing the field dependence of the e-h pair amplitudes C_n introduced in Eq. (24). It demonstrates the prominent D-I crossover in the X-GS, a much weaker D-I coupling in the X-ES, and a very quick transition from symmetric coupling to D-I coupling, seen in the WFs of both X-GS and X-ES.

Figure 8 shows the field dependence of the optical transition energies E_X and binding energies E_b of X-GS and X-ES, as well as their in-plane exciton Bohr radii $r_B = \sqrt{\langle\rho^2\rangle}$ and the radiative linewidths Γ_R. The latter are calculated via Eq. (27) assuming $d_{cv} = 0.6$ nm.[38,39] While all these parameters for the X-GS change dramatically when the EF increases from 2 kV/cm to 8 kV/cm, the X-ES remains practically unaffected. The X-GS energy exhibits a considerable Stark shift, for $F >$ 6 kV/cm almost linear in F [Fig. 8(a)], due to the electron-hole separation typical for the indirect exciton. The X-ES in turn has a very weak field dependence due to a much smaller dipole moment of the direct exciton, but in a larger range of the EF values, the X-ES transition energy is also red shifted (by 12 meV at $F = 100$ kV/cm), as a result of an EF-induced electron-hole separation within the same QW.

The X-GS binding energy, $E_b = E_1^{(0)} - E_X$, drops from 8 meV to 4 meV [Fig. 8(b)], as a result of the transition from direct to indirect Coulomb coupling. For the X-ES the binding energy is defined as the energy distance from X-ES to its own continuum onset: $E_b = E_2^{(0)} - E_X$. This is done because the lowest-energy pair state, $e1h1$, has a negligible (for $F >$ 1 kV/cm) contribution to the X-ES, and, thus, this exciton state remains bound even though its energy E_X is higher than the first continuum onset $E_1^{(0)}$. The X-ES binding energy is almost unchanged, as the EF has no effect on the direct nature of this state. The Bohr radius [Fig. 8(c)] is fully correlated with the

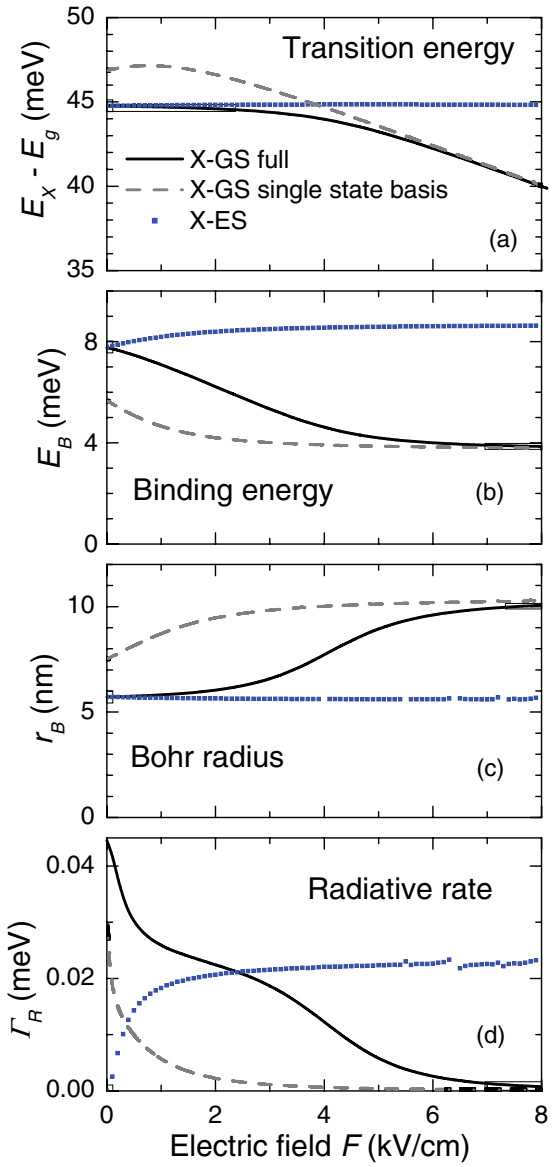

FIG. 8. (Color online) (a) Optical transition energy E_X, (b) binding energy E_b, (c) in-plane Bohr radius $r_B = \sqrt{\langle \rho^2 \rangle}$, and (d) radiative rate Γ_R of the exciton ground state X-GS (solid lines) and excited state X-ES (full squares) as functions of the electric field F. Dashed lines are the single-state-basis calculation of the X-GS.

binding energy, increasing with the EF almost by a factor of 2 for the X-GS and showing no change for the X-ES.

The D-I crossover is accompanied by a dramatic decrease of the radiative linewidth of the X-GS (proportional to its oscillator strength); see Fig. 8(d). This happens because the EF makes the electron-hole separation larger, reducing the overlap of the electron and hole WFs. The X-ES, in turn, being strictly dark at $F = 0$, becomes bright in a finite EF, and its linewidth quickly increases with the EF up to the half of the maximum linewidth of the X-GS. Further increase of the EF does not change the X-ES radiative rate much but Γ_R experiences some influence of higher ESs; see the fluctuations in Fig. 8(d).

To reproduce some previous simulations[21] and to compare them with our full calculation, we have restricted our basis to the electron and hole GSs only, neglecting any ESs quantized in the growth direction. In other words, we have taken into account only one e-h pair state, $e1h1$, choosing $N = 1$ in the expansion Eq. (12). This single-state basis (SSB) calculation shows considerably different results compared to the full calculation in all four plots in Fig. 8; see the dashed curves. The reason for such a difference is obvious: Figure 7(a) clearly demonstrates the importance of taking into account higher e-h pair states for a proper description of the D-I crossover of the X-GS and, in particular, the role in such a crossover of state $e2h1$, which is missing in the SSB calculation. This state is a direct pair state (at least for $F > 0.5$ kV/cm), so neglecting it in the X-GS calculation, as done, e.g., in Ref. 21, underestimates the exciton binding energy by a factor of 1.5 and the exciton radiative linewidth by an order of magnitude. Nevertheless, at larger EFs ($F > 10$ kV/cm) the SSB model adequately describes the properties of the X-GS as such an indirect exciton state is strongly dominated by $e1h1$.

Finally, Fig. 9 shows our simulation for an asymmetric $In_{0.08}Ga_{0.92}As/GaAs/In_{0.1}Ga_{0.9}As$ (10 nm/4 nm/10 nm) CQW structure used in Ref. 8. As expected, the energy spectra are asymmetric with respect to the EF direction. In the right part of the exciton energy spectrum [Fig. 9(a)], at around 16 kV/cm, a Coulomb-induced anticrossing is observed, which is similar to that seen in Fig. 4 at $F = 5$ kV/cm. The physical mechanism that causes this anticrossing is essentially the same as in the case of symmetric CQWs, but the anticrossing takes place at much higher values of the electric field. This is because at around $F = 12$ kV/cm (4–5 kV/cm below the anticrossing) the applied EF almost compensates the asymmetry in the conduction band structure, and, thus, at this value of F the properties of the asymmetric CQW can resemble those of the symmetric CQW at $F = 0$. In fact, a repulsion of the electron subbands is seen in Fig. 9(b) as well as a formation of symmetric and antisymmetric electronic states, as is clear from the inset in Fig. 9(a).

B. Indirect exciton lifetime

A CQW exciton can escape from the system using the following two major channels: It can either recombine by emitting a photon or the electron and/or hole can tunnel through the external barrier with the help of the EF. We concentrate here on the X-GS only, and, combining both channels together, the total exciton lifetime takes the form

$$\frac{1}{\tau} = \frac{1}{\tau_R} + \frac{1}{\tau_T}, \tag{28}$$

where $\tau_R = \hbar/(2\Gamma_R)$ is the exciton radiative lifetime. As for the tunneling time τ_T, we take into account the lowest pair state only. This is a valid approximation because when other pair states contribute to the X-GS and, thus, can have some effect on the exciton tunneling, its lifetime is strongly dominated by the radiative channel as can be seen in Fig. 10. In particular, the tunneling lifetime $\tau_T = \hbar/(\Gamma_1^e + \Gamma_1^h)$ is much longer than the radiative one up to $F = 80$ kV/cm. The D-I crossover of the X-GS is accompanied by a monotonous growth of its radiative lifetime, in accordance with Fig. 8(d). Indeed, a direct exciton has a short lifetime because the carriers are in the same well, so they can easily recombine. Increasing the

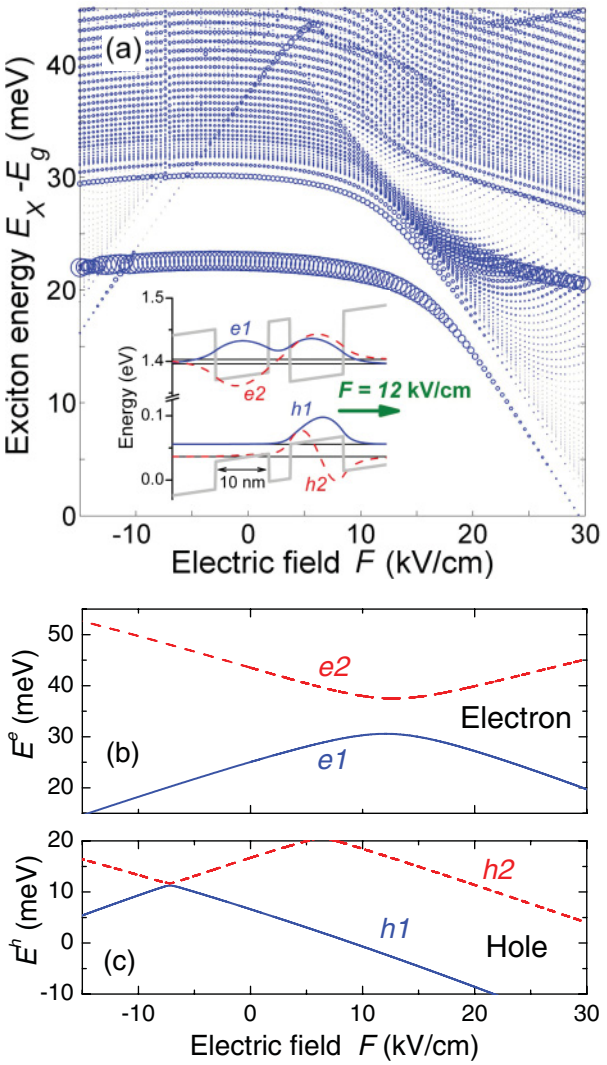

FIG. 9. (Color online) (a) Exciton energies and oscillator strengths (circle area) and [(b) and (c)] electron and hole subbands in asymmetric $In_{0.08}Ga_{0.92}As/GaAs/In_{0.1}Ga_{0.9}As$ (10 nm/4 nm/10 nm) CQW structure as functions of the applied electric field F. The inset shows CQW band structure and direction of the electric field, as well as the electron and hole wave functions and energy levels of the ground and first excited quantized states for $F = 12$ kV/cm.

electron-hole separation leads to a dramatic increase of the radiative lifetime. The probability of the electron and hole tunneling also increases with EF. At some point the tunneling time becomes comparable to the radiative lifetime and then starts to dominate. We have also compared the calculated radiative lifetime for the X-GS with the experimental results taken from Ref. 30 where the low-temperature excitonic photoluminescence was measured in 8–4–8-nm $GaAs/Al_{0.33}Ga_{0.67}As$ CQWs. The inset to Fig. 10 demonstrates a quantitative agreement between the experiment and the present theory.

C. Absorption spectrum

We also calculate the exciton absorption coefficient in a 8–4–8-nm $GaAs/Al_{0.33}Ga_{0.67}As$ CQW at different frequencies

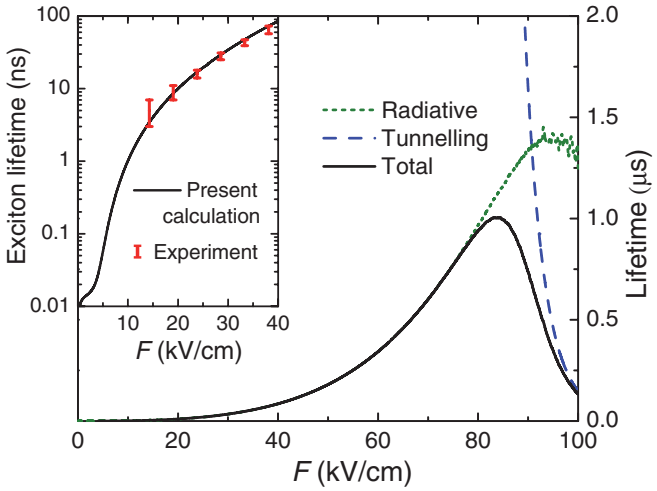

FIG. 10. (Color online) Radiative (dotted curve), tunneling (dashed curve), and total lifetimes (solid curve) of the exciton ground state X-GS as functions of the applied electric field. (Inset) Logarithmic plot of the X-GS total lifetime in comparison with measured photoluminescence decay times (error bars) extracted from Ref. 30.

of the incoming light. Using the Lorentzian model of absorbing oscillators[37,40] and leaving out a common prefactor, the absorption of the exciton with zero in-plane momentum takes the form

$$\alpha(\omega) = \sum_{\nu} \Gamma_{R,\nu} \frac{\Gamma_{R,\nu}}{(\hbar\omega - E_\nu)^2 + \Gamma_{R,\nu}^2}, \tag{29}$$

where the index ν labels all possible excitonic states calculated in the theory and E_ν and $\Gamma_{R,\nu}$ stand for their energies and radiative linewidths.

Figure 11(a) shows the absorption spectrum calculated using Eq. (29) and in-plane exciton confinement radius $R = 800$ nm. All lines in the absorption have very narrow radiative widths (<0.1 meV) which are calculated according to Eqs. (26) and (27). The Lorentzian model, however, has an obvious artifact: Although the spectrum properly reproduces the linewidths, all lines have the same peak height, and the fact that not all of them are seen in Fig. 11(a) is due only to the resolution of the plot. To improve on this and also to take into account the effect of inhomogeneous line broadening in realistic CQW structures, we make a Gauss convolution of the spectrum: $A(\omega) = \int_{-\infty}^{\infty} \alpha(\omega')g(\omega - \omega')d\omega'$ with a normalized Gauss function $g(\omega) = (\Delta\sqrt{\pi})^{-1}e^{-\omega^2/\Delta^2}$. The convoluted spectrum with the full width at half maximum (FWHM) $2\sqrt{\ln 2}\Delta = 0.2$ meV is shown in Fig. 11(b). All lines now have almost the same width but their peak maxima now reflect the optical strength of the corresponding exciton states.

The two lowest excitonic states, X-GS and X-ES, are well resolved in the spectrum up to $F = 5$ kV/cm. Then the indirect exciton X-GS loses its optical activity. The bright direct X-ES line superimposes with higher ESs and discretized continuum of the indirect exciton, all line merging up together at higher EFs.

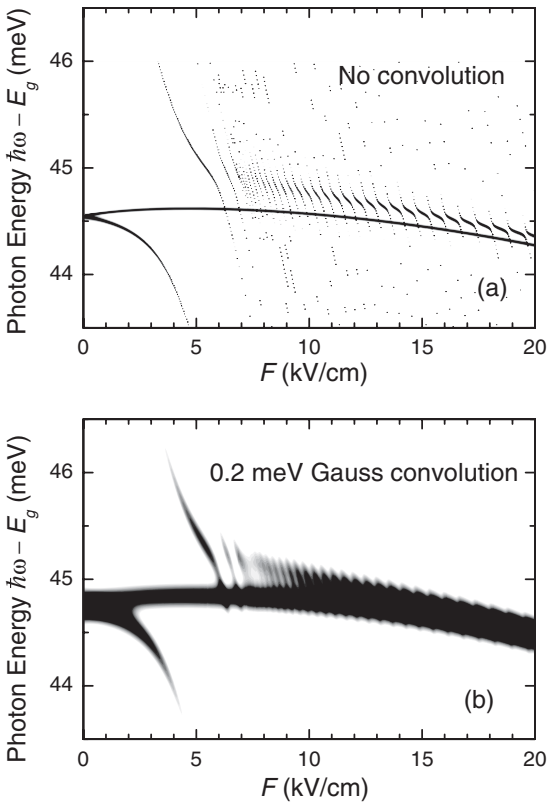

FIG. 11. (a) Electric field dependence of the full excitonic absorption spectrum. (b) The same spectra convoluted with a Gaussian function with 0.2-meV full width at half maximum.

D. Numerical code

We have provided a freely available online software[31] that calculates the optical properties of the direct and indirect excitons in a CQW structure in a perpendicular EF. The software has a user-friendly interface and produces an on-screen output of the requested calculation as well as a PDF version of the same data and plots. For the input, the user has an option either to choose a symmetric AlGaAs CQW, inserting the required structural parameters (L_b, L_w, and x), or an asymmetric InGaAs CQW, or to take other semiconductor CQW by inserting its structural and material parameters. The value of the EF is also needed for the input. In this numerical code, we use four basis states for the exciton WF, taking into account only the ground and the first excited states for the electron and hole. The exciton confinement radius is set to $R = 200$ nm. The transition energies and the oscillator strengths of exciton excited states are also included in the output file. The absorption spectrum is calculated with 0.1 meV FWHM Gaussian convolution.

IV. CONCLUSIONS

We have studied the effect the electric field has on excitonic states in AlGaAs and InGaAs CQWs. To do this we have developed an efficient numerical approach which is based on expanding the exciton wave function into uncorrelated electron-hole pair states and solving in the real space a matrix Schrödinger equation for the CQW exciton. Using this approach we have calculated the energies and the wave functions of exciton states in the CQW and studied their optical properties in the presence of electric field, by addressing such important parameters of the exciton as its binding energy, Bohr radius, radiative and tunneling times, and optical absorption spectrum. While we are able to calculate a large number of exciton states, we have concentrated on two most important ones, the exciton ground state X-GS and the brightest excited state X-ES. We have shown that the Coulomb coupling between direct and indirect pair states leads to a prominent effect in the presence of the electric field: a direct-to-indirect crossover of the X-GS. At the same time, the properties of the X-ES remain almost unchanged. Finally, we have calculated the exciton lifetime which consists of two main components, radiative and tunneling times, and shown that the latter reduces the total lifetime at higher electric fields.

ACKNOWLEDGMENTS

We thank Jeremy Baumberg, Wolfgang Langbein, and Roland Zimmermann for useful discussions and Richard Frewin for technical support of the Web site. K. S. acknowledges support of the Royal Thai Government. L. M. acknowledges FP7-REGPOT-2008-1, Project BIOSOLENUTI no. 229927 for financial support.

*Present address: Department of Physics, University of Crete, 71003 Heraklion, Crete, Greece.
†On leave from General Physics Institute RAS, Moscow, Russia; egor.muljarov@astro.cf.ac.uk

[1] L. V. Butov, C. W. Lai, A. L. Ivanov, A. C. Gossard, and D. S. Chemla, Nature **417**, 47 (2002).
[2] G. Grosso, J. Graves, A. T. Hammack, A. A. High, L. V. Butov, M. Hanson, and A. C. Gossard, Nat. Photon. **3**, 577 (2009).
[3] A. T. Hammack, L. V. Butov, J. Wilkes, L. Mouchliadis, E. A. Muljarov, A. L. Ivanov, and A. C. Gossard, Phys. Rev. B **80**, 155331 (2009).
[4] A. G. Winbow *et al.*, Phys. Rev. Lett. **106**, 196806 (2011).
[5] Z. Vörös, D. W. Snoke, L. Pfeiffer, and K. West, Phys. Rev. Lett. **97**, 016803 (2006).
[6] Z. Vörös, D. W. Snoke, L. Pfeiffer, and K. West, Phys. Rev. Lett. **103**, 016403 (2009).
[7] G. J. Schinner, E. Schubert, M. P. Stallhofer, J. P. Kotthaus, D. Schuh, A. K. Rai, D. Reuter, A. D. Wieck, and A. O. Govorov, Phys. Rev. B **83**, 165308 (2011).
[8] G. Christmann, A. Askitopoulos, G. Deligeorgis, Z. Hatzopoulos, S. I. Tsintzos, P. G. Savvidis, and J. J. Baumberg, Appl. Phys. Lett. **98**, 081111 (2011).
[9] H.-J. Polland, L. Schultheis, J. Kuhl, E. O. Göbel, and C. W. Tu, Phys. Rev. Lett. **55**, 2610 (1985).

[10]C. C. Phillips, R. Eccleston, and S. R. Andrews, Phys. Rev. B **40**, 9760 (1989).
[11]J. E. Golub, K. Kash, J. P. Harbison, and L. T. Florez, Phys. Rev. B **41**, 8564 (1990).
[12]A. Alexandrou, J. A. Kash, E. E. Mendez, M. Zachau, J. M. Hong, T. Fukuzawa, and Y. Hase, Phys. Rev. B **42**, 9225 (1990).
[13]S. Charbonneau, M. L. W. Thewalt, E. S. Koteles, and B. Elman, Phys. Rev. B **38**, 6287 (1988).
[14]Y. J. Chen, E. S. Koteles, B. S. Elman, and C. A. Armiento, Phys. Rev. B **36**, 4562 (1987).
[15]S. R. Andrews, C. M. Murray, R. A. Davies, and T. M. Kerr, Phys. Rev. B **37**, 8198 (1988).
[16]J. H. Kim, T. W. Kim, and K. H. Yoo, Appl. Surf. Sci. **240**, 452 (2005).
[17]H. Q. Le, J. J. Zayhowski, and W. D. Goodhue, Appl. Phys. Lett. **50**, 1518 (1987).
[18]D. Ahn and S. L. Chuang, Phys. Rev. B **34**, 9034 (1986).
[19]E. J. Austin and M. Jaros, Appl. Phys. Lett. **47**, 274 (1985); Phys. Rev. B **31**, 5569 (1985).
[20]J. A. Kash, E. E. Mendez, and H. Morkoç, Appl. Phys. Lett. **46**, 173 (1985).
[21]I. Galbraith and G. Duggan, Phys. Rev. B **40**, 5515 (1989).
[22]T. Kamizato and M. Matsuura, Phys. Rev. B **40**, 8378 (1989).
[23]J. Lee, M. O. Vassell, E. S. Koteles, and B. Elman, Phys. Rev. B **39**, 10133 (1989).
[24]M. M. Dignam and J. E. Sipe, Phys. Rev. B **43**, 4084 (1991).
[25]I. Linnerud and K. A. Chao, Phys. Rev. B **49**, 8487 (1994).
[26]Y. Takahashi, Y. Kato, S. S. Kano, S. Fukatsu, Y. Shiraki, and R. Ito, J. Appl. Phys. **76**, 2299 (1994).
[27]J. Soubusta, R. Grill, P. Hlídek, M. Zvára, L. Smrčka, S. Malzer, W. Geißelbrecht, and G. H. Döhler, Phys. Rev. B **60**, 7740 (1999).
[28]M. H. Szymanska and P. B. Littlewood, Phys. Rev. B **67**, 193305 (2003).
[29]S. C. Arapan and M. A. Liberman, J. Lumin. **112**, 216 (2005).
[30]L. V. Butov, A. Imamoglu, A. V. Mintsev, K. L. Campman, and A. C. Gossard, Phys. Rev. B **59**, 1625 (1999).
[31][http://CQWExciton.cf.ac.uk/].
[32]J. H. Davies, *The Physics of Low-Dimensional Semiconductors* (Cambridge University Press, Cambridge, 1998).
[33]L. W. Molenkamp, R. Eppenga, G. W.' t Hooft, P. Dawson, C. T. Foxon, and K. J. Moore, Phys. Rev. B **38**, 4314 (1988).
[34]M. Abramowitz and I. A. Stegun, *Handbook of Mathematical Functions (with Formulas, Graphs, and Mathematical Tables)* (Dover, New York, 1965).
[35]A. J. F. Siegert, Phys. Rev. **56**, 750 (1939).
[36]R. M. More, Phys. Rev. A **4**, 1782 (1971).
[37]L. C. Andreani, in *Confined Electrons and Photons: New Physics and Applications*, edited by E. Burstein and C. Weisbuch (Plenum Press, New York, 1995).
[38]E. Rosencher and B. Vinter, *Optoelectronics* (Cambridge University Press, Cambridge, 2002).
[39]P. G. Eliseev, H. Li, A. Stintz, G. T. Liu, T. C. Newell, K. J. Malloy, and L. F. Lester, Appl. Phys. Lett. **77**, 262 (2000).
[40]R. J. Elliott, Phys. Rev. **108**, 1384 (1957).